AIP | Applied Physics Letters

Self-powered, hybrid antenna-magnetoresistive sensor for magnetic field detection

R. Macedo, F. A. Cardoso, S. Cardoso, P. P. Freitas, J. Germano et al.

Citation: Appl. Phys. Lett. **98**, 103503 (2011); doi: 10.1063/1.3562340
View online: http://dx.doi.org/10.1063/1.3562340
View Table of Contents: http://apl.aip.org/resource/1/APPLAB/v98/i10
Published by the American Institute of Physics.

Self-powered, hybrid antenna-magnetoresistive sensor for magnetic field detection

R. Macedo,[1,a)] F. A. Cardoso,[1] S. Cardoso,[1] P. P. Freitas,[1] J. Germano,[2] and M. S. Piedade[2]

[1]*Institute for Nanosciences and Nanotechnologies, INESC–MN, R. Alves Redol 9, 1000-029 Lisbon, Portugal and Department of Physics, Instituto Superior Técnico, Universidade Técnica de Lisboa, 1049-001 Lisbon, Portugal*

[2]*INESC–ID, R. Alves Redol 9, 1000-029 Lisbon, Portugal and Department of Electrical Engineering, Instituto Superior Técnico, Universidade Técnica de Lisboa, 1049-001 Lisbon, Portugal*

(Received 10 September 2010; accepted 8 February 2011; published online 8 March 2011)

A self-powered hybrid sensor integrating a resonant antenna with a magnetoresistive spin valve sensor was microfabricated. The device is activated by a radiofrequency (rf) external electromagnetic source. This hybrid sensor is capable of detecting dc and ac external magnetic fields in the thermal noise regime. For an excitation rf field of 17 dB m at 130 MHz, the sensitivity to a transverse magnetic field normalized by the current induced in the device was 812 V $(T A)^{-1}$ for dc magnetic field detection and 918 V $(T A)^{-1}$ for the ac field measurement. © *2011 American Institute of Physics*. [doi:10.1063/1.3562340]

Magnetoresistive (MR) (Refs. 1–3) sensors have been widely used for various field detection applications in picotesla to microtesla range.[4,5] These applications take advantage of the high magnetic field sensitivity of MR sensors, small dimensions, integration capability, and reduced cost. Several emerging applications of embedded systems such, as sensor networks and biomedical implants, require advances in wireless technology and low power electronics. To enable the wireless ability, these sensors require an integrated power supply, normally with a brief lifetime. They alternatively can harvest the surrounding energy and convert it into usable energy.[6,7] This work presents a strategy to fabricate a self-powered hybrid sensor for dc and ac magnetic field detection.

This hybrid sensor assembly includes a microfabricated three-loop resonant antenna (the receiving antenna) in series with a spin valve sensor (SV), which has a constriction (CT) in parallel (Fig. 1). The CT is located on top and electrically isolated from the SV [Fig. 1(b)]. In the presence of a driving rf field an electromotive force is induced in the antenna, generating an ac current. As the SV and the CT are in parallel, part of this ac current biases the SV the other portion passes through the CT creating an ac field that will be sensed by the SV located underneath.

The resulting voltage output for a linear SV sensor when this hybrid device is excited by a driving sinusoidal rf field of frequency f_1, is given by the following equation:[8]

$$V_{SV} = R^0_{SV} I^0_{SV} \sin(2\pi f_1 t) - (\Delta R/2B^{eff}_k) I^0_{SV} I^0_{CT} (\alpha/2) \times [1 - \cos(4\pi f_1 t)]\}, \quad (1)$$

where R^0_{SV} is the SV resistance at zero field, $\Delta R = R_{AP} - R_P$ (R_{AP} and R_P are the SV resistances in the antiparallel and parallel states), B^{eff}_k is the free layer effective anisotropy field dominated by the free layer demagnetizing field, I^0_{SV} and I^0_{CT} are the amplitude of the currents passing through the SV and CT, respectively. α is a geometric factor relating the field at the sensor with the current in the CT ($B_{CT} = \alpha I_{CT}$).

The response of the SV, in the hybrid device, to an external in plane (to the antenna loop) and transverse (to the SV sensor length) dc (B^{ext}_{dc}) or AC [$B^{ext}_{ac}(f_2)$] field, is given by Eq. (2a) as follows:

$$V_{SV} = R^0_{SV} I^0_{SV}(f_1) - (\Delta R/2B^{eff}_k) I^0_{SV}(f_1)[\alpha I_{CT}(f_1) + B^{ext}_{dc} + B^{ext}_{ac}(f_2)]. \quad (2a)$$

Computing Eq. (2a), four peaks are expected in the SV sensor voltage spectrum

- At f_1 with amplitude $[R^0_{SV} - (\Delta R/2B^{eff}_k) B^{ext}_{dc}] I^0_{SV}$ (2b)
- At $2f_1$, with amplitude $0.5(\Delta R/2B^{eff}_k) I^0_{SV} I^0_{CT} \alpha$ (2c)
- Two peaks at $f_1 \pm f_2$, with amplitude $0.5(\Delta R/2B^{eff}_k) I^0_{SV} B^{ext}_{ac}$. (2d)

An external transverse dc field can be detected by measuring the amplitude variation in the peak at f_1. The external transverse ac field is measured acquiring the amplitude of the side peaks at $f_1 \pm f_2$. Information on the exciting rf field is obtained from the SV sensor response at $2f_1$. Devices based on magnetoresistive sensors using similar signal multiplica-

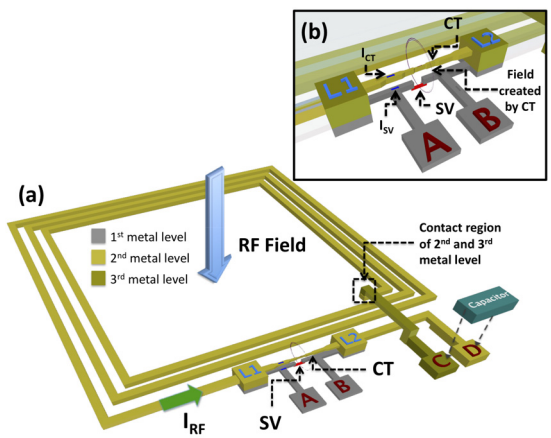

FIG. 1. (Color online) (a) Schematic of the hybrid device incorporating a three turn antenna and a SV sensor. (b) Detail of the CT of the antenna on top and in parallel with the SV.

a)Electronic mail: rmacedo@inesc-mn.pt.

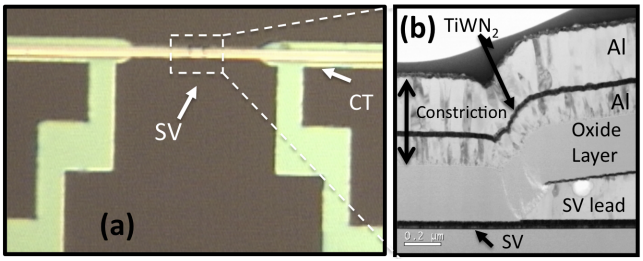

FIG. 2. (Color online) (a) Optical image of the microfabricated device, showing the region of the CT on top of the SV in the inset on the right. (b) Transmission electron microscopy view of a focused-on-beam cross section through the sensor/lead/CT area.

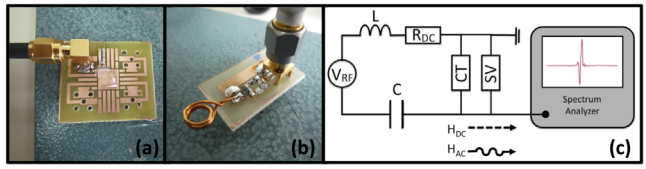

FIG. 3. (Color online) (a) Chip with hybrid sensor wirebonded to a PCB platform. (b) Activation/excitation antenna. (c) Schematic of the experiment to perform the dc and ac field detection.

tion and with outputs varying with external magnetic fields were already proposed.[9]

Device fabrication started with a top pinned SV stack ion beam deposition (Nordiko 3600 system with a base pressure of 4×10^{-8} Torr) onto a glass substrate. The deposited stacks have the following structure (thickness in nanometers): glass/Ta 2/NiFe 2.5/CoFe 2.5/Cu 2/CoFe 2.5/MnIr 6/Ta 2, where CoFe, NiFe and MnIr, stand for $Co_{80}Fe_{20}$, $Ni_{80}Fe_{20}$, and $Mn_{77}Ir_{23}$ in atomic percent. A 15 nm thick $Ti_{10}W_{90}(N)$ passivation layer was then deposited by magnetron sputtering. The easy axis of the free and pinned layers were set parallel to each other by applying a 10 mT aligning field during deposition. In this top pinned configuration, no annealing was required to set the exchange field. Bulk samples were microfabricated (using optical lithography, ion milling, and lift off) down to dimensions of 2.5×17 μm^2 (the distance between the two sputtered $Al_{98.5}Si_1Cu_{0.5}300/Ti_{10}W_{90}N_230$ electrical leads, the first metal level, is 7 μm) in order to linearize the sensor by shape anisotropy. The fabricated SVs show a two-probe magnetoresistance signal of 5.6%, resistance ranging from 92.3 to 97.5 Ω, and a sensitivity ($\Delta R/2B_k^{eff}$) of 2.6 Ω/m T.

After SV sensor and leads definition, a 300 nm thick sputtered Al_2O_3 passivation, layer was deposited, leaving four vias open (by lift-off); two to enable a later contact to the metal CT layer (L1 and L2 in Fig. 1), and the other two for sensor output readout (A and B in Fig. 1).

A flat square $Al_{98.5}Si_1Cu_{0.5}$ $150/Ti_{10}W_{90}N_2$ $15/Al_{98.5}Si_1Cu_{0.5}$ $300/Ti_{10}W_{90}N_2$ 15, three-loop antenna was then defined by optical lithography and lift-off. The antenna comprises three turns and internal area of 2×2 mm^2 (each leg of the antenna has a width of 50 μm; and a spacing of 10 μm). On top of the SV, the antenna width was reduced to 4 μm on a length of 500 μm forming the CT region, as shown in Fig. 2. In this step, one of the contacts of the hybrid device is defined [contact D in Fig. 1(a)]. A final sputtered Al_2O_3 passivation layer (300 nm thick) is deposited all over the device, with a via left open by lift-off in the extremity of the inner loop [in Fig. 1(a)]. A third metallization level $Al_{98.5}Si_1Cu_{0.5}$ $300/Ti_{10}W_{90}N_2$ 15, is used to bring the inner loop contact to the external loop contact region [see contact C in Fig. 1(a)]. The microfabricated wafer was diced into individual dies and wire-bonded to a printed circuit board (PCB) [Fig. 3(a)]. The final device, composed of the flat squared metallic antenna in series with the parallel of SV and CT, shows a resistance (measured between contacts C and D) of approximately 110 Ω. The resistance value found for the antenna was 73.4 Ω (measured between contacts A and C) and for the SV//CT was 37.57 Ω (measured between contacts A and C). The impedance response versus frequency was measured between terminals C and D using a network/spectrum analyzer (HP 4195A). From this measurement, the resistance at dc, the inductance, and capacitance of the hybrid device were determined (107 Ω, 56 nH, and 1 pF, respectively). In order to turn the device into a resonant antenna at 130 MHz a 21 pF capacitor was mounted between C and D [Fig. 1(a)] effectively closing the antenna loop. At this frequency, the device is in the thermal noise regime, enabling a maximum signal-to-noise ratio.

The activation of the hybrid device is done using a home-made three turns, 5 mm diameter antenna connected to a rf source (HP8645A) which by Ampere's law creates a rf field [Fig. 3(b)]. In order to guarantee the matching of impedances a 50 Ω surface mount resistor was connected in series with the excitation antenna.

This excitation antenna is placed on top and centered with the receiving antenna. The rf current induced in the hybrid device (I_{HYB}) depends on the distance d between the two elements. The rf driving frequency was 130 MHz (the resonance value for the device) with amplitude of 17 dB m, resulting in a current of 31 mA passing through the excitation antenna and a field of 23.6 μT at its center.

The hybrid MR-Antenna was tested as a dc and ac magnetic field self-powered sensor. For the dc field detection experiment two coils connected to a dc power source (GW GPC-3020D) were used to create a dc magnetic field. The value of d was 2.5 ± 0.5 mm, leading to a rf field and I_{HYB} of 2.78 μT and 0.25 mA, respectively. Assuming this value, the calculated current biasing (I_{SV}^0) of the sensor was 98 μA. In the case of the ac field experiment an electromagnet powered by a function generator (Agilent 33220A), connected to an amplifier with a gain of 10 was used. Due to the setup geometry, d was 1.5 cm ±0.5 mm for this experiment. The rf field and I_{HYB} were 34.95 nT and 3.11 μA, respectively, leading to I_{SV}^0 of 1.22 μA. The external dc or ac field created was placed in-plane and transverse to the SV sensor length and its output observed in a HP 4195A in spectrum analyzer mode [Fig. 3(c)].

Figure 4(a) shows the spectrum of the SV sensor from 100 to 300 MHz (no external field applied). The two expected peaks at f_1 and $2f_1$ are observed. The amplitude measured for the peak at f_1 was 10.94 mV and the expected value was 9.34 mV [Eq. (2b)]. Using Eq. (2c), a theoretical value of 2.75 μV was found for the $2f_1$ peak ($I_{CT}=I_{HYB}-I_{SV}^0=152$ μA, $\alpha=0.14$ T A^{-1}). However, the experimental value of this peak is 66.3 μV. This discrepancy can be explained considering the existence of harmonics coming from the rf source. As expected, the f_1 peak amplitude varies by applying a 1 mT dc transverse field [inset of Fig. 4(a)].

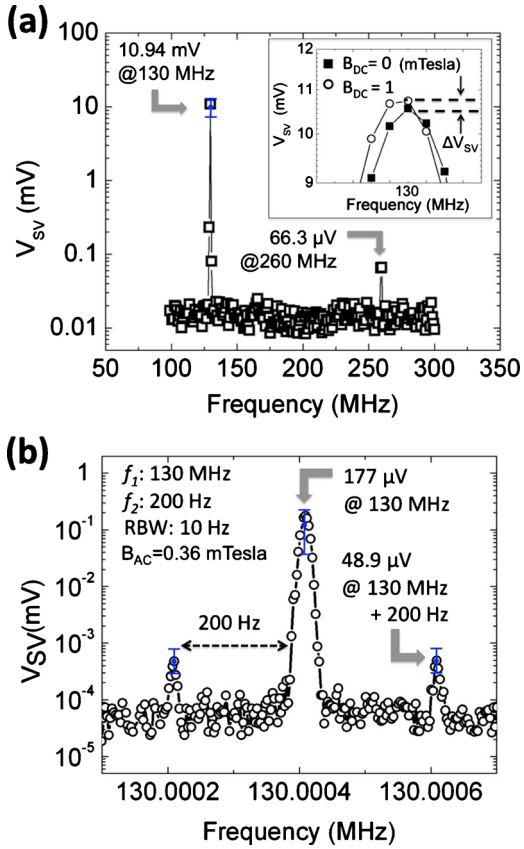

FIG. 4. (Color online) (a) Spectrum of the SV output of the experiment for dc field detection, where the peaks at f_1 and $2f_1$ are observed. The inset shows the peak at f_1 in detail for two different B_{dc} fields. (b) Spectrum of the SV sensor acquired in the experiment to detect ac fields. The peaks at f_1 (130 MHz) and $f_1 \pm f_2$ (130 MHz ± 200 Hz) are observed. The calculated values and correspondent error bars are also depicted.

Figure 4(b) shows the spectrum of the SV sensor when a 0.36 mT rms ac magnetic field at 200 Hz is applied. As predicted, three peaks are observed at f_1 and at $f_1 \pm f_2$, with amplitudes of 117 μV (f_1) and 48.9 μV ($f_1 \pm f_2$,), respectively. The calculated values for these peaks were 177 μV and 57 μV [using Eqs. (2b) and (2d), respectively]. The deviations from the theoretical value of the f_1 peak for both dc and ac experiments and of $f_1 \pm f_2$ peaks in the ac experiment can be explained by the error in the measurement of d.

The SV sensor output at $f_1 \pm f_2(V_{SV})$ obtained in the ac experiment and the variation in the output value of the SV sensor at $f_1(\Delta V_{SV})$ acquired in the dc experiment were plotted in Fig. 5. Equations (2c) and (2d) were used to plot the theoretical values of these values. An increase in the amplitude of the two signals with the external magnetic field is observed while the SV sensor is in its linear range. In the SV sensor saturation a constant value is obtained. This behavior is a clear indication of the sensing capability of the hybrid device presented in this work. From Fig. 5, a sensitivity of 203 mV/T and 1.12 mV/T was determined for the dc and ac field detection experiments, respectively. These values correspond to detection limits of 6.2 $nT/Hz^{1/2}$ and 1.125 $\mu T/Hz^{1/2}$ for dc and ac fields, respectively. The formerly sensitivity values can be normalized by the I_{HYB} values in each case, leading to sensitivity values independent of

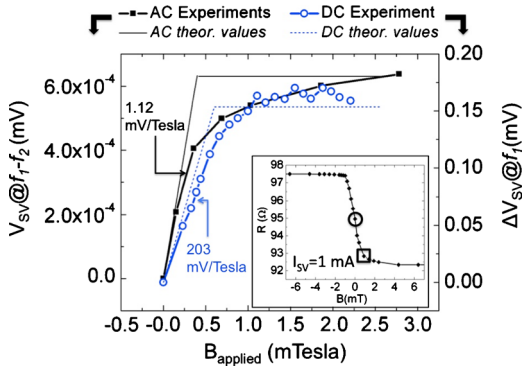

FIG. 5. (Color online) Variation in the SV output at f_1 (acquired in the dc experiment) and the amplitude variation in the peaks at $f_1 \pm f_2$ (obtained for the ac experiment) as function of the amplitude of the external field applied. The theoretical curves calculated for both experiments are also shown (dashed line for dc and straight line for ac). The inset shows the transfer curve of the SV sensor.

the setup geometry. For the dc experiment the value of the normalized sensitivity is 812 V $(T A)^{-1}$ and for the ac case this value is 918 V $(T A)^{-1}$.

The next challenge for this work is related with the appearance of a dc component, which should have the same amplitude as the peak at 2f, when the device is excited by a rf field. This feature opens up additional types of applications for the MR-Antenna device.

In conclusion, a hybrid self-powered rf powered device, integrating a SV sensor and a rf receiving antenna was microfabricated. This hybrid device shows the capability of sensing dc and ac external transverse magnetic fields. The fabricated device, driven by an excitation field at 130 MHz and 17 dB m, shows a normalized sensitivity of 812 V $(T A)^{-1}$ for the dc field experiment and 918 V $(T A)^{-1}$ for the ac field case. This device can further optimized, for example, by reducing the resistance of the receiving antenna or increasing the MR sensor sensitivity, for instance, by using a magnetic tunnel junction sensor (which show sensitivities ten times higher than the SV) instead of a SV sensor.

R. Macedo wishes to thank FCT for the Ph.D. Grant (Grant No. SFRH/BD/30670/2006). INESC MN acknowledges FCT funding through the Associated Lab-Instituto de Nanotecnologias.

[1]J. E. Lenz, Proc. IEEE **78**, 973 (1990).
[2]D. J. Mapps, Sens. Actuators, A **59**, 9 (1997).
[3]R. S. Popovic, J. A. Flanagan, and P. A. Besse, Sens. Actuators, A **56**, 39 (1996).
[4]R. C. Chaves, P. P. Freitas, B. Ocker, and W. Maass, Appl. Phys. Lett. **91**, 102504 (2007).
[5]A. Guedes, S. B. Patil, P. Wisniowski, V. Chu, J. P. Conde, and P. P. Freitas, IEEE Trans. Magn. **44**, 2554 (2008).
[6]J. B. Kurt Roth, ASHRAE J. **50**, 84 (2008).
[7]R. Vijay and H. C. Pai, Proceedings of 2006 International Symposium on Low Power Electronics and Design (ACM, Tegernsee, Bavaria, Germany, 2006).
[8]P. P. Freitas, R. Ferreira, S. Cardoso, and F. Cardoso, J. Phys.: Condens. Matter **19**, 165221 (2007).
[9]A. A. Tulapurkar, Y. Suzuki, A. Fukushima, H. Kubota, H. Maehara, K. Tsunekawa, D. D. Djayaprawira, N. Watanabe, and S. Yuasa, Nature (London) **438**, 339 (2005).